Strain rate dependency of 3D printed metamaterials

Ondřej Jiroušek

Department of Mechanics and Materials
Czech Technical University in Prague

University of Padova
October 25, 2022

Introduction






Concrete 3D printing by Federico Diaz, FEM by CTU

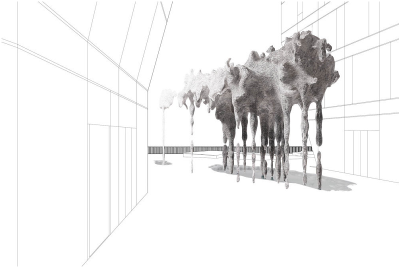



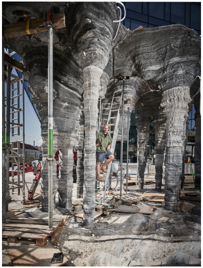

Concrete 3D printing, CTU Klokner's institute




3D printed materials, structures, cellular materials, auxetics

Motivation

Cellular materials, 3D printed structures, auxetics

- natural cellular materials (trabecular bone research, wood, etc.)
- metal foams (closed-cell, open-cell), hybrid foams
- auxetic materials (metamaterials)
- 3D printed (SLS, SLM) structures
- IPCs (cellular core, strain-rate sensitive filling)

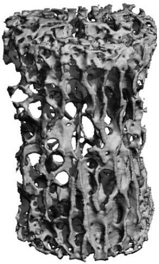
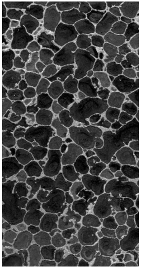
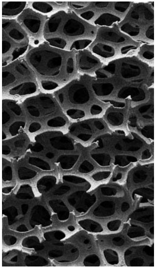
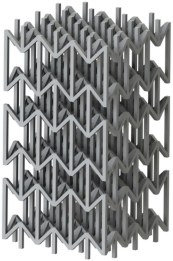

Strain rate dependency?

Stress-strain relationship, 2D correlation, static tests

Principles of DIC in 2D:

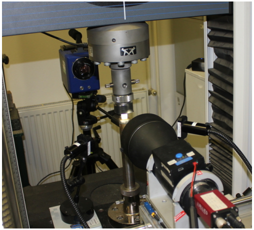

Loaded sample, surface pattern:

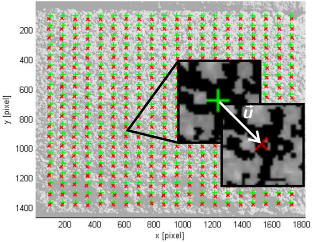

Features tracking: a) single point

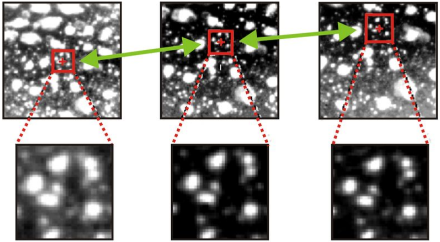

b) entire sample area

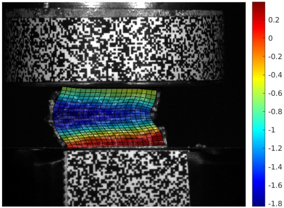

Principles of DIC in 2D

Displacements: Linear deformation is used to link a position (x, y) in the reference image with the corresponding position (x_0, y_0) in the deformed image:

$$x^{'} - x = u + \frac{\partial u}{\partial x}\mathrm{d}x + \frac{\partial u}{\partial y}\mathrm{d}y$$
$$y^{'} - y = v + \frac{\partial v}{\partial x}\mathrm{d}y + \frac{\partial v}{\partial y}\mathrm{d}y$$

Remark: The transformation of initial reference subset points to the current configuration is typically constrained to a *linear, first order transformation*. General form of the deformation vector, w_{2D}:

$$w_{2D} = \left(u, v, \frac{\partial u}{\partial x}, \frac{\partial u}{\partial y}, \frac{\partial v}{\partial x}, \frac{\partial v}{\partial y}\right)$$

Affine transformation

Affine transform is composed of a linear transform and a translation transform.

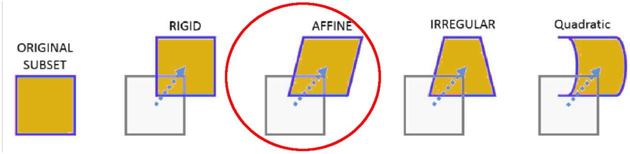

In 2D space the transform can be expressed as

$$\begin{bmatrix} x' \\ y' \end{bmatrix} = \begin{bmatrix} a_{11} & a_{12} \\ a_{21} & a_{22} \end{bmatrix} \begin{bmatrix} x \\ y \end{bmatrix} + \begin{bmatrix} t_x \\ t_y \end{bmatrix}$$

where $\begin{bmatrix} a_{11} & a_{12} \\ a_{21} & a_{22} \end{bmatrix}$ is a real matrix, $\begin{bmatrix} t_x \\ t_y \end{bmatrix}$ stands for the translation vector.
Six-parameter affine transform:

$$\begin{bmatrix} x' \\ y' \end{bmatrix} = \begin{bmatrix} a_{11} & a_{12} & t_x \\ a_{21} & a_{22} & t_y \end{bmatrix} \begin{bmatrix} x \\ y \\ 1 \end{bmatrix} = \boldsymbol{A} \begin{bmatrix} x \\ y \\ 1 \end{bmatrix}$$

where $\boldsymbol{A} = \begin{bmatrix} a_{11} & a_{12} & t_x \\ a_{21} & a_{22} & t_y \end{bmatrix}$ represents *affine transform matrix*.

Correlation coeeficient:

To measure the similarity between two images (two extracted subsets)

a) cross-correlation coefficient

$$C_{CC} = \frac{\sum_{(i,j)} \left(f(x_{ref,i}, y_{ref,j}) - f_m\right)\left(g(x_{cur,i}, y_{cur,j}) - g_m\right)}{\sqrt{\sum_{(i,j)} \left(f(x_{ref,i}, y_{ref,j}) - f_m\right)^2 \sum_{(i,j)} \left(g(x_{cur,i}, y_{cur,j}) - g_m\right)^2}}$$

f and g ... reference and current image functions (grayscale value at specified (x, y) point

f_m and g_m ... mean grayscale values of the final reference and current subset, respectively, defined by:

$$f_m = \frac{\sum_{(i,j)} f(x_{ref,i}, y_{ref,j})}{n}$$

$$g_m = \frac{\sum_{(i,j)} g(x_{cur,i}, y_{cur,j})}{n}$$

Good match when C_{CC} is close to 1.

Correlation coeeficient:
b) least-square cc

$$C_{LS} = \sum_{(i,j)} \left[\frac{f(x_{ref,i}, y_{ref,j}) - f_m}{\sum_{(i,j)} (f(x_{ref,i}, y_{ref,j}) - f_m)^2} - \frac{g(x_{cur,i}, y_{cur,j}) - g_m}{\sum_{(i,j)} (g(x_{cur,i}, y_{cur,j}) - g_m)^2} \right]^2$$

f and g ... reference and current image functions (grayscale value at specified (x, y) point
f_m and g_m ... mean grayscale values of the final reference and current subset, respectively, defined by:

$$f_m = \frac{\sum_{(i,j)} f(x_{ref,i}, y_{ref,j})}{n}$$

$$g_m = \frac{\sum_{(i,j)} g(x_{cur,i}, y_{cur,j})}{n}$$

Good match when C_{LS} is close to 0.

Lukas-Kanade algorithm

Lukas-Kanade algorithm
goal is to minimize:

$$\sum_x \left[I\left(W(x;p)\right) - T(x)\right]^2$$

with respect to a vector of parameters $p = (p_1, p_2, ..., p_n)^T$.
Additive image alignment:

$$\sum_x \left[I\left(W(x;p+\Delta p)\right) - T(x)\right]^2$$

First order Taylor expansion:

$$\sum_x \left[I\left(W(x;p)\right) + \nabla I \frac{\partial W}{\partial p}\Delta p - T(x)\right]^2$$

This is a least square problem with solution:

$$\Delta p = \sum_x H^{-1}\left[\nabla I \frac{\partial W}{\partial p}\right]^T \left[T(x) - I\left(W(x;p)\right)\right]$$

where H is the (n, n) *Hessian matrix*:

$$H = \sum_x \left[\nabla I \frac{\partial W}{\partial p}\right]^T \left[\Delta I \frac{\partial W}{\partial p}\right]$$

Lukas-Kanade algorithm

Additive algoritm: iterate until the estimates of the parameters p converge:

1. Warp I with $W(x;p)$ to compute $I(W(x;p))$;
2. Compute the error image $T(x) - I(W(x;p))$;
3. Warp the gradient of image I to compute ∇I;
4. Evaluate the Jacobian $\frac{\partial W}{\partial p}$;
5. Compute the Hessian matrix using $H = \sum_x \left[\nabla I \frac{\partial W}{\partial p}\right]^T \left[\Delta I \frac{\partial W}{\partial p}\right]$;
6. Compute Δp using $\Delta p = \sum_x H^{-1} \left[\nabla I \frac{\partial W}{\partial p}\right]^T [T(x) - I(W(x;p))]$;
7. Update the parameters $p \leftarrow p + \Delta p$.

The estimate of the parameters p varies from iteration to iteration.

Two main approaches: Global (FE-based) and Local:

- subset-based vs finite-element-based local-global approach
- use of higher-order elements possible (T6 and Q8)
- linear vs quadratic mapping in affine transformation
- strains calculated by (global) differentiation vs using shape-functions
- compatible strain fields

- pixel level - SSD criterion
- sub-pixel level - ZNSSD criterion

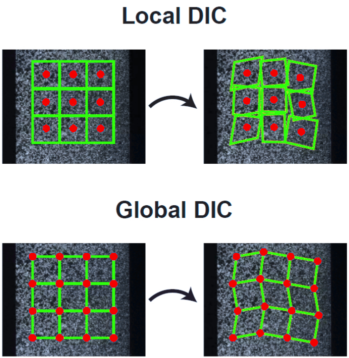

Strain evaluation:

From the displacements, strains are calculated using deformation gradient tensor F:
Green-Lagrange deformation tensor:

$$\mathbf{E} = \begin{bmatrix} E_{xx} & E_{xy} \\ E_{xy} & E_{yy} \end{bmatrix} = \mathbf{F^T F} - \mathbf{I} = \frac{1}{2}\left[(\nabla_{\mathbf{X}} \mathbf{u})^T \nabla_{\mathbf{X}} \mathbf{u} - \mathbf{I}\right]$$

in components:

$$E_{xx} = \frac{\partial u}{\partial x} + \frac{1}{2}\left[\left(\frac{\partial u}{\partial x}\right)^2 + \left(\frac{\partial v}{\partial x}\right)^2\right]$$

$$E_{yy} = \frac{\partial v}{\partial y} + \frac{1}{2}\left[\left(\frac{\partial u}{\partial y}\right)^2 + \left(\frac{\partial v}{\partial y}\right)^2\right]$$

$$E_{xy} = \frac{1}{2}\left(\frac{\partial u}{\partial y} + \frac{\partial v}{\partial x}\right) + \frac{1}{2}\left[\frac{\partial u}{\partial x}\frac{\partial u}{\partial y} + \frac{\partial v}{\partial x}\frac{\partial v}{\partial y}\right]$$

DIC application – material testing, fracture mechanics

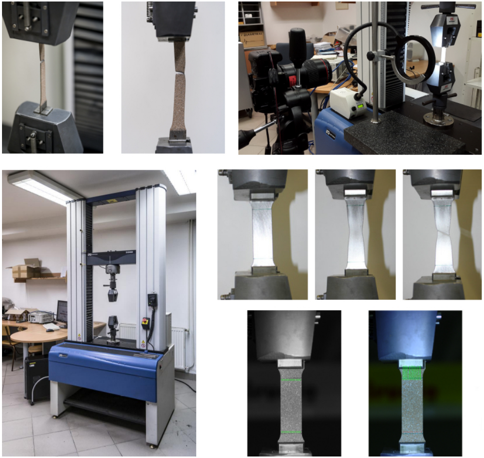

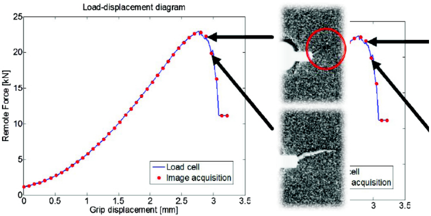

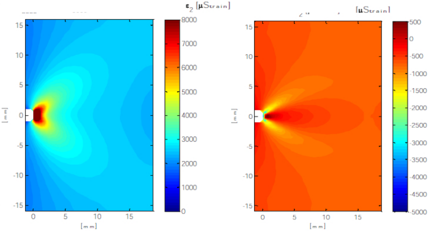

Local based approach is sufficient

DIC results expamples – static experiments global FE-based approach:: E_{yy}

tkdh-bd-13: Beam-Direct variant

- proper adaptive remeshing of the grid needed for large deformations

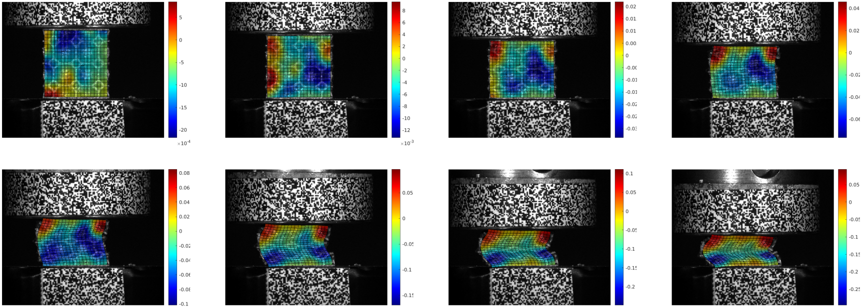

DIC results expamples – static experiments

tkdh-bs-13: Beam-Stem variant

- proper adaptive remeshing of the FE grid needed for large deformations

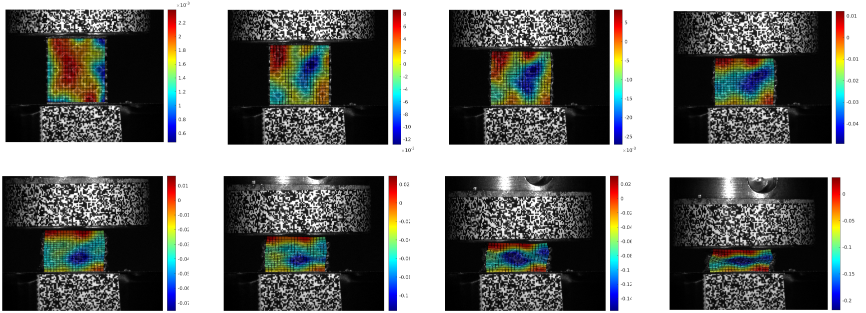

DIC results expamples – static experiments

tkdh-fd-13: Facet-direct variant

- proper adaptive remeshing of the FE grid needed for large deformations

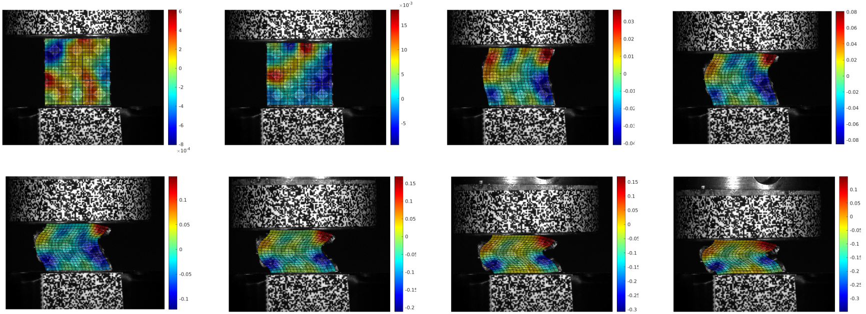

DIC results expamples – static experiments

tkdh-fs-13: Facet-stem variant

- proper adaptive remeshing of the FE grid needed for large deformations

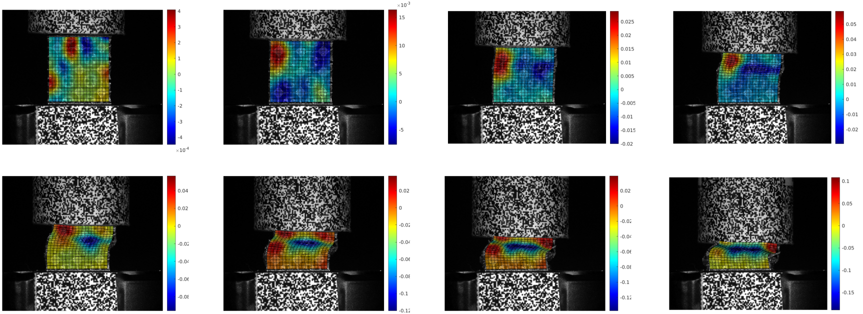

Structural characterization – micro Computed Tomography

microfocus X-ray tomography

- microfocus X-ray source (spot size 1 μm or even smaller)
- X-ray detector (flat panel, photon counting and particle tracking pixel detectors)
- rotating table with fixed specimen
- beam-hardening, cone-beam reconstruction, other issues (e.g. thermal drift)

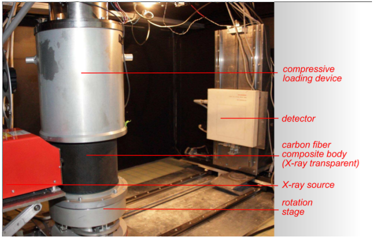

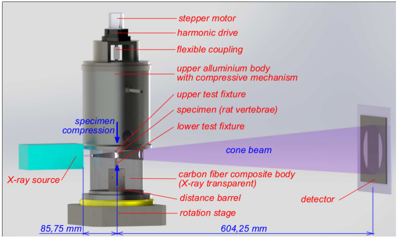

Cone beam reconstruction

- different from (basic) inverse radon transformation
- accounts fully for the geometry of the beam
- utilization of GPU processing is of great advantage (easy parallelization)

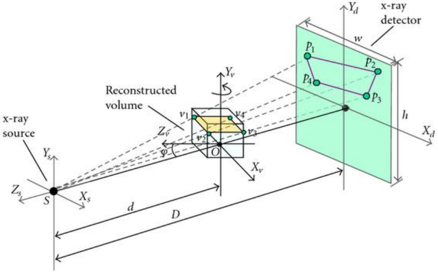

Figure: Geometry of back projection. The slice under reconstruction has each filtered X-ray image projected onto it by projective texture mapping.

Digital Volume Correlation - principle

- extension of DIC (Digital Image Correlation) in 3D space
- correlation coefficient for the best fit between subvolumes
- nonlinear optimization technique to maximize the correlation coefficient.

$$w_{3D} = \left(u, v, w, \frac{\partial u}{\partial x}, \frac{\partial u}{\partial y}, \frac{\partial u}{\partial z}, \frac{\partial v}{\partial x}, \frac{\partial v}{\partial y}, \frac{\partial v}{\partial z}, \frac{\partial w}{\partial x}, \frac{\partial w}{\partial y}, \frac{\partial w}{\partial z} \right)$$

The cross-correlation coefficient C_{CC} is defined:

$$C_{CC} = \frac{\sum_{(i,j,k)} \left(f(x_{ref,i}, y_{ref,j}, z_{ref,k}) - f_m \right) \left(g(x_{cur,i}, y_{cur,j}, z_{ref,k}) - g_m \right)}{\sqrt{\sum_{(i,j,k)} \left(f(x_{ref,i}, y_{ref,j}, , z_{ref,k}) - f_m \right)^2 \sum_{(i,j,k)} \left(g(x_{cur,i}, y_{cur,j}, z_{ref,k}) - g_m \right)^2}}$$

f and g ... reference and current image functions (grayscale value at specified (x, y, z) point
f_m and g_m ... mean grayscale values of the final reference and current subset, respectively, defined by:

$$f_m = \frac{\sum_{(i,j,k)} f(x_{ref,i}, y_{ref,j}, z_{ref,k})}{n}; \quad g_m = \frac{\sum_{(i,j,k)} g(x_{cur,i}, y_{cur,j}, z_{cur,k})}{n}$$

Good match when C_{CC} is close to 1.

Calculation of displacement, strain tensors

Direct use of coefficients of linear affine transformation (between the undeformed and deformed state):

- components of displacement vector (u, v, w)
- components of gradient tensor $\frac{\partial u}{\partial x}, \frac{\partial u}{\partial y}, \frac{\partial u}{\partial z}, \frac{\partial v}{\partial x}, \frac{\partial v}{\partial y}, \frac{\partial v}{\partial z}, \frac{\partial w}{\partial x}, \frac{\partial w}{\partial y}, \frac{\partial w}{\partial z}$.

Use: deformation gradient tensor **F**:

$$F_{ij} = x_{i,j} = \frac{\partial x_i}{\partial X_j} = \begin{bmatrix} \frac{\partial x_1}{\partial X_1} & \frac{\partial x_1}{\partial X_2} & \frac{\partial x_1}{\partial X_3} \\ \frac{\partial x_2}{\partial X_1} & \frac{\partial x_2}{\partial X_2} & \frac{\partial x_2}{\partial X_3} \\ \frac{\partial x_3}{\partial X_1} & \frac{\partial x_3}{\partial X_2} & \frac{\partial x_3}{\partial X_3} \end{bmatrix}$$

where X is used to define the *undeformed* (reference) configuration, and x defines the *deformed* (current) configuration.
Displacement u of any point can be defined simply as $u = x - X$.

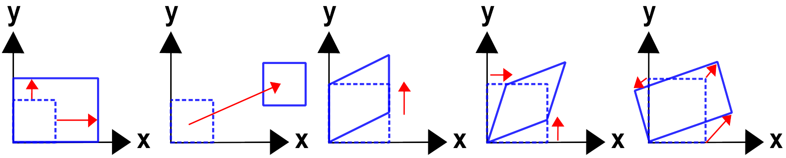

Affine transformation in 3D

translation

$$T_t = \begin{pmatrix} 1 & 0 & 0 & t_x \\ 0 & 1 & 0 & t_y \\ 0 & 0 & 1 & t_z \\ 0 & 0 & 0 & 1 \end{pmatrix}$$

rotation

$$T_r = \begin{pmatrix} \cos\ \theta & -\sin\ \theta & 0 & 0 \\ \sin\theta & \cos\theta & 0 & 0 \\ 0 & 0 & 1 & 0 \\ 0 & 0 & 0 & 1 \end{pmatrix}$$

scale

$$T_s = \begin{pmatrix} s_x & 0 & 0 & 0 \\ 0 & s_y & 0 & 0 \\ 0 & 0 & s_z & 0 \\ 0 & 0 & 0 & 1 \end{pmatrix}$$

shear

$$T_h = \begin{pmatrix} 1 & 0 & sh_x & 0 \\ 0 & 1 & sh_y & 0 \\ 0 & 0 & 1 & 0 \\ 0 & 0 & 0 & 1 \end{pmatrix}$$

Green-Lagrange deformation tensor:

$$\mathbf{E} = \begin{bmatrix} E_{xx} & E_{xy} & E_{xz} \\ E_{xy} & E_{yy} & E_{yz} \\ E_{xz} & E_{yz} & E_{zz} \end{bmatrix} = \mathbf{F^T F} - \mathbf{I}$$

$$\begin{aligned}
E_{xx} &= \frac{\partial u}{\partial X} + \frac{1}{2}\left[\left(\frac{\partial u}{\partial X}\right)^2 + \left(\frac{\partial v}{\partial X}\right)^2 + \left(\frac{\partial w}{\partial X}\right)^2\right] \\
E_{yy} &= \frac{\partial v}{\partial Y} + \frac{1}{2}\left[\left(\frac{\partial u}{\partial Y}\right)^2 + \left(\frac{\partial v}{\partial Y}\right)^2 + \left(\frac{\partial w}{\partial Y}\right)^2\right] \\
E_{zz} &= \frac{\partial w}{\partial Z} + \frac{1}{2}\left[\left(\frac{\partial u}{\partial Z}\right)^2 + \left(\frac{\partial v}{\partial Z}\right)^2 + \left(\frac{\partial w}{\partial Z}\right)^2\right] \\
E_{xy} &= \frac{1}{2}\left(\frac{\partial u}{\partial Y} + \frac{\partial v}{\partial X}\right) + \frac{1}{2}\left[\frac{\partial u}{\partial X}\frac{\partial u}{\partial Y} + \frac{\partial v}{\partial X}\frac{\partial v}{\partial Y} + \frac{\partial w}{\partial X}\frac{\partial w}{\partial Y}\right] \\
E_{xz} &= \frac{1}{2}\left(\frac{\partial u}{\partial Z} + \frac{\partial w}{\partial X}\right) + \frac{1}{2}\left[\frac{\partial u}{\partial X}\frac{\partial u}{\partial Z} + \frac{\partial v}{\partial X}\frac{\partial v}{\partial Z} + \frac{\partial w}{\partial X}\frac{\partial w}{\partial Z}\right] \\
E_{yz} &= \frac{1}{2}\left(\frac{\partial v}{\partial Z} + \frac{\partial w}{\partial Y}\right) + \frac{1}{2}\left[\frac{\partial u}{\partial Y}\frac{\partial u}{\partial Z} + \frac{\partial v}{\partial Y}\frac{\partial v}{\partial Z} + \frac{\partial w}{\partial Y}\frac{\partial w}{\partial Z}\right]
\end{aligned}$$

Graphical illustration of the DVC principle

Tracking of features in a sequence of image data:

- image intensities converted to 3-D matrix
- moving with the base image ROI in the deformed image (3-D)

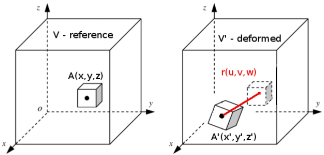

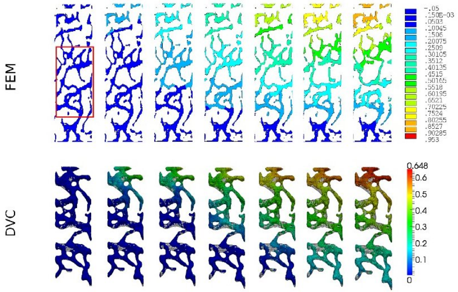

Jiroušek, O., Jandejsek, I., & Vavřík, D. Evaluation of strain field in microstructures using micro-CT and digital volume correlation. *Journal of Instrumentation*, **6**(01), C01039, 2011. **IF 3.148**

Jandejsek, I., Jiroušek, O., Vavřík, D. Precise strain measurement in complex materials using digital volumetric correlation and time lapse micro-CT data. *Procedia Engineering* 10 ,pp. 1730-1735, 2011.

Jiroušek, O. Strain measurements in time-lapse microtomography of trabecular bone using digital volume correlation method. *Proceedings of the 7th IASTED International Conference on Biomedical Engineering, BioMED 2010*, 2, pp. 72-75, 2010. *Procedia Engineering*, 10, pp. 1730-1735, 2011.

Tetra - from known nodal displacements $\{r\}$:

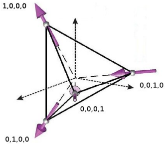

$$\mathbf{E} = \begin{bmatrix} E_{xx} & E_{xy} & E_{xz} \\ E_{xy} & E_{yy} & E_{yz} \\ E_{xz} & E_{yz} & E_{zz} \end{bmatrix} = \mathbf{F}^{\mathbf{T}}\mathbf{F} - \mathbf{I}$$

Volumetric coordinates ξ_i mapping :

$$\xi_i = \frac{V_i}{V} \qquad \textit{for } i = 1, 2, 3, 4 \tag{1}$$

Natural coordinates ξ_i defined as volumetric ratio, i.e. for i=1:

$$\xi_1 = \frac{V_1}{V} = \frac{\begin{vmatrix} 1 & 1 & 1 & 1 \\ x & x_2 & x_3 & x_4 \\ y & y_2 & y_3 & y_4 \\ z & z_2 & z_3 & z_4 \end{vmatrix}}{\begin{vmatrix} 1 & 1 & 1 & 1 \\ x_1 & x_2 & x_3 & x_4 \\ y_1 & y_2 & y_3 & y_4 \\ z_1 & z_2 & z_3 & z_4 \end{vmatrix}} \tag{2}$$

For linear tetrahedra:

$$N_i = \xi_i$$

The strain-nodal displacement matrix B is given by derivatives of $N_i = \xi_i$ :: $B = \partial N$:
Then the strain tensor is computed from the nodal displacements given by the correlation results:

$$\{\varepsilon_{ij}\} = [B]\{r\}$$

voxel vs tetra FE models – source for DVC

tetrahedral ⇒ voxel model

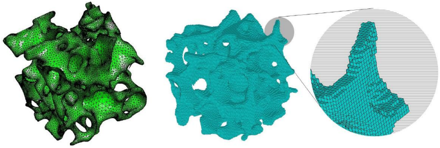

DVC measured displacements compared to FEM calculated ones

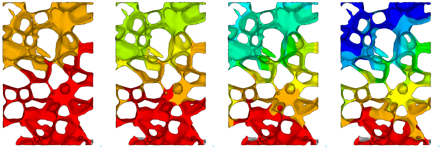

- each voxel (spatial pixel) directly converted into linear hexahedra
- gradual loading according to the experiment
- material properties: linear elastic, based on nanoindentation tests $\surd$

KEY ADVANTAGES:

Direct comparison of measured and calculated results
Important for assessment of material constants of advanced material models (e.g. visco-elasto-plastic with damage)
Large strain analysis (plasticity, post-yield behavior)

Advantage: direct FE model – comparison

- 708,872 elements
- 196,675 nodes $\Rightarrow$ 1,258,773 nodes (quadratic shape functions)
- displacement boundary conditions
- results compared in a smaller sub-volume

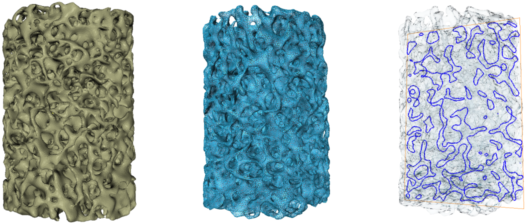

Jiroušek, O., Zlámal, P., Kytýř, D., & Kroupa, M. (2011). Strain analysis of trabecular bone using time-resolved X-ray microtomography. *Nuclear Instruments and Methods in Physics Research Section A: Accelerators, Spectrometers, Detectors and Associated Equipment*, **663(1), S148–S151.**

DVC Example – Al and Ti metal foam testing

- modified design of the experimental device
- higher toughness, use of high-strength composite material

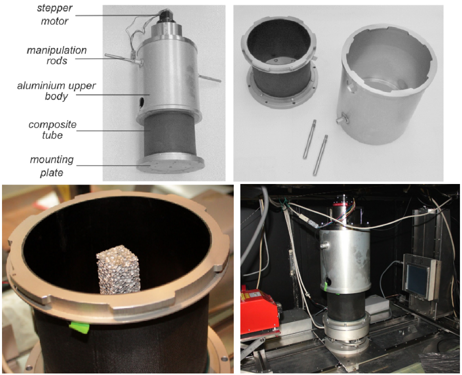

microFE model of microstructure

- voxel-based modelling, intensity-based thresholding
- large number of elements needed (to capture the pore imperfections)

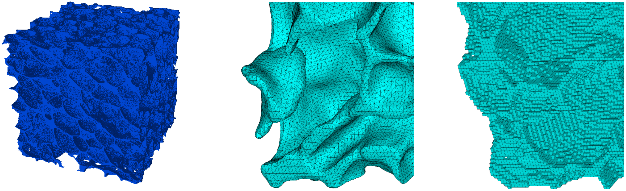

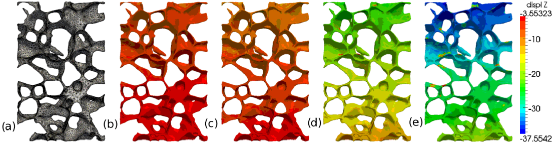

DVC example – Hybrid foams

- Aluminum foams (AlSi7Mg0.3) by M-pore, Dresden, Germany
- Pore sizes of 10 and 30 ppi,
- Plated by DC or PED with nanonickel particles

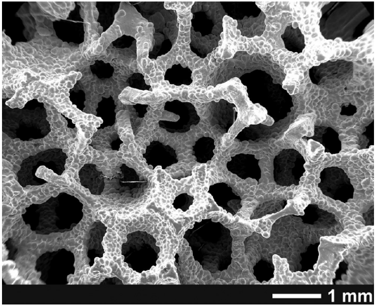

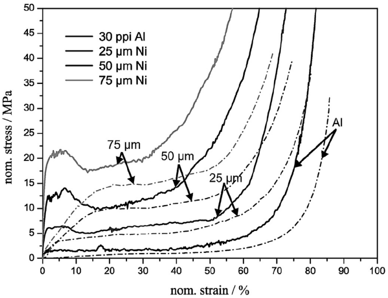

A. Jung, E. Lach, S. Diebels, New hybrid foam materials for impact protection, International Journal of Impact Engineering, 64 (2014) 30–38.

Dual energy X-ray imaging

- Necessary to distinguish between Al and Ni layers
- To quantify the quality of coating
- Two X-ray sources with different energies

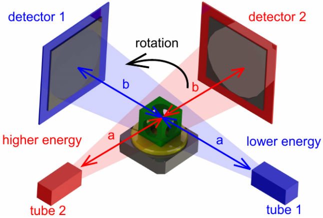

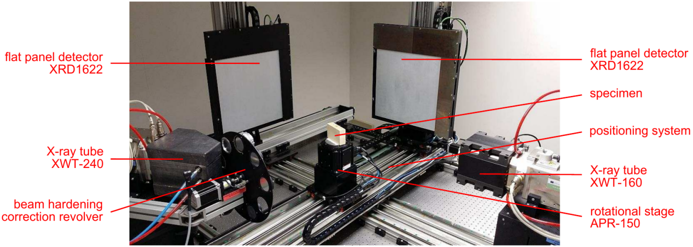

Dual energy X-ray imaging - RESULTS

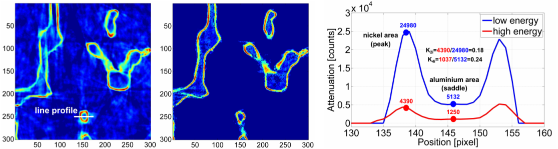

(a) (b) (c)

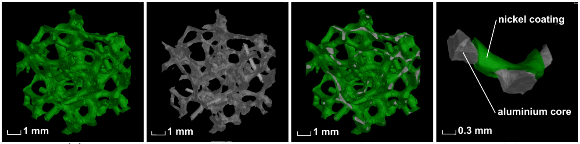

(a) (b) (c) (d)

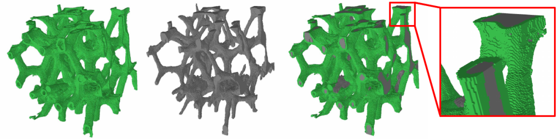

(a) (b) (c) (d)

Fíla, T., Kumpová, I., Koudelka, P., Zlámal, P., Vavřík, D., Jiroušek, O., Jung, A. Dual-energy X-ray micro-CT imaging of hybrid Ni/Al open-cell foam Journal of Instrumentation 11(1), 2016.

Hybrid PU/Ni foam - micro-CT experiments

- Dual and single energy micro-CT experiments

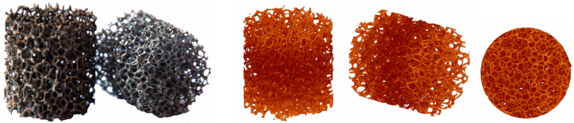

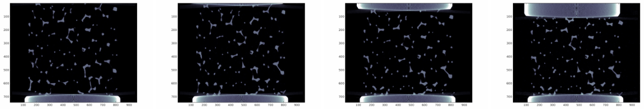

- Stress-strain curves, QS loading. Four distinct parts: (a) proportional elastic behaviour, (b) peak stress, (c) plateau region (d) strain hardening region

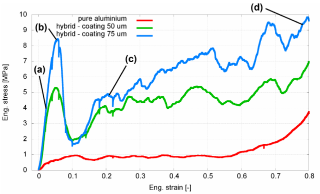

Hybrid foams - micro-CT experiments

- Dual and single energy micro-CT experiments

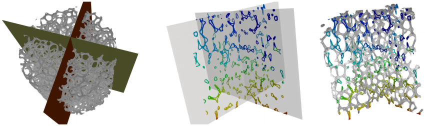

- Results of DVC

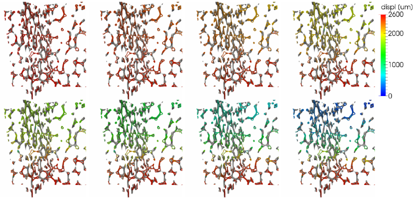

Hybrid foam - micro-CT experiments

- Visualization of the 3D data

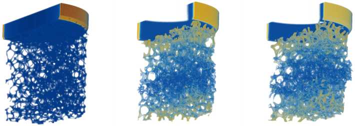

- Detail of the results calculated in the sub-volume of the pure Al sample microstructure (100 $\times$ 100 $\times$ 100 pixels). First row - displacements, second row - strains. Note the highly localized strains captured by DVC.

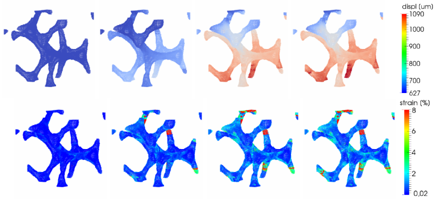

T. Fíla, O. Jiroušek, A. Jung , I. Kumpová Identification of strain fields in pure Al and hybrid Ni/Al metal foams using X-ray micro-tomography under loading *Journal of Instrumentation*, 2016.

Hybrid Al/Ni foam - numerical simulations

- Model the strain rate dependency
- Simulate the microgravitational effects

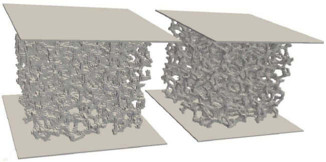

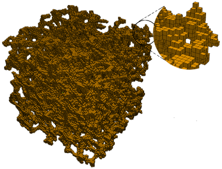

- Specific energy absorption capacities up to the densification point as function of the Ni coating thickness, expressed per volume (lower curves) and per density (upper curves)
- Comparison of the stress-strain diagrams for quasi-static and dynamic compression tests (dashed lines: quasi-static 5×10^{-3} s^{-1}, compact lines: dynamic 5000 s^{-1})

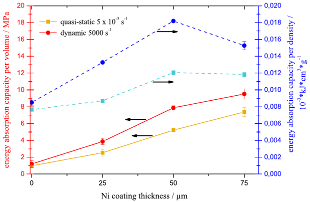

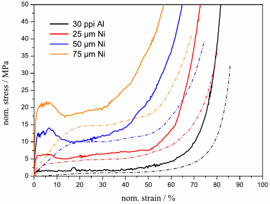

Hybrid Al/Ni foam - numerical simulations

- Explicit dynamics code Europlexus
- Hexahedral elements, covered with a layer of shell elements representing the coating (only modelling of uniform coating thickenss possible)
- Large analysis, proper modelling of self contact needed

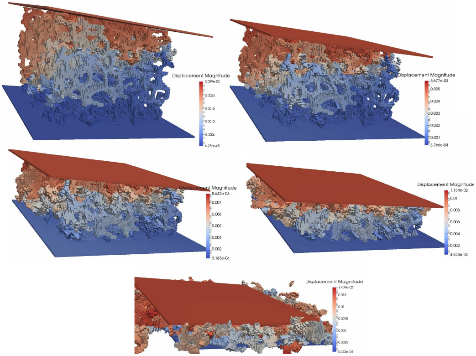

- Micro model as virtual testing laboratory, μCT measurements performed to determine the microstructure of the foams
- Micro-inertia effects (microstructure) are crucial for strain-rate dependency
- Simulations show a strain-rate sensitivity for the alumminium foams

A. Jung, M. Larcher, O. Jiroušek, et al Strain-rate Dependence for Ni/Al Hybrid Foams *DYMAT*, 2015.

High strain-rate testing - SHPB/OHPB

Split Hopkinson Pressure Bar (SHPB)

- Established method for dynamic testing at high strain-rates
- Strain-rate range $100 - 10,000\,\mathrm{s}^{-1}$
- Principle - wave propagation theory in slender bars
- Strain-gages for wave measurements
- Valid test - dynamic equilibrium

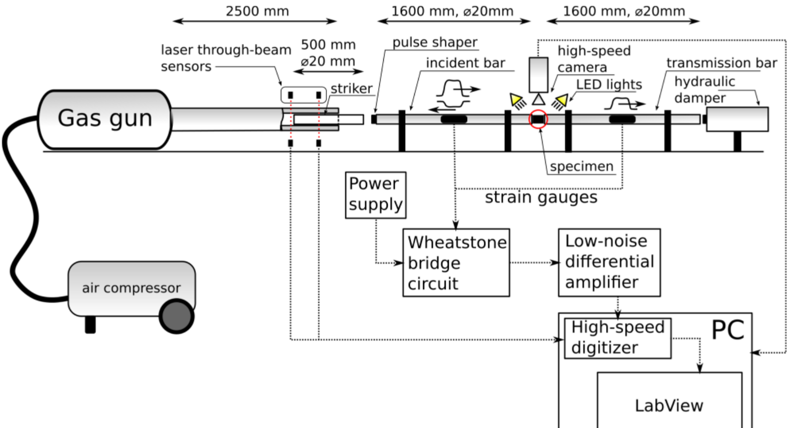

Split Hopkinson Pressure Bar (SHPB)

- Established method for dynamic testing at high strain-rates
- Strain-rate range $100 - 10,000\,\mathrm{s}^{-1}$
- Principle - wave propagation theory in slender bars
- Strain-gages for wave measurements
- Valid test - dynamic equilibrium

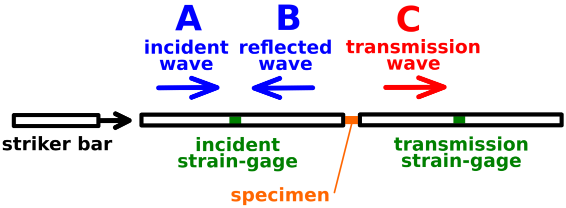

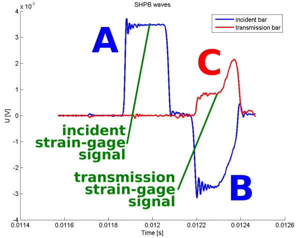

Strain rate limitations

Compression experiments

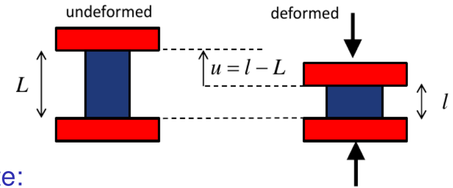

Nominal strain rate:

$$\varepsilon_{\text{eng}} = \frac{l}{L} - 1 \implies \dot{\varepsilon}_{\text{eng}} = \frac{\dot{l}}{L} = \frac{\dot{u}}{L}$$

True strain rate:

$$\varepsilon = \ln\left[1 + \varepsilon_{\text{eng}}\right] \implies \dot{\varepsilon} = \frac{\dot{\varepsilon}_{\text{eng}}}{1 + \varepsilon_{\text{eng}}}$$

Equivalent strain rate:

$$\dot{\varepsilon} = \frac{|\dot{\varepsilon}_{\text{eng}}|}{1 + \varepsilon_{\text{eng}}}$$

Quasi-static equilibrium

Static force:

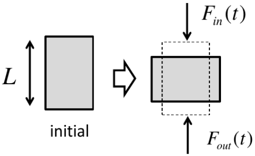

Force equivalency for all times:

$$F_{IN}(t) = F_{OUT}(t)$$

Strain at the end of the experiment: $\varepsilon_{\max}$
Average strain rate (over time): $\dot{\varepsilon}_{\mathrm{av}}$
Experiment total time (duration):

$$T = \frac{\varepsilon_{\max}}{\dot{\varepsilon}_{\mathrm{av}}}$$

Example 1:

$$\varepsilon_{\max} = 0.1$$

$$\dot{\varepsilon}_{\mathrm{av}} = 500/s$$

$$T = \frac{\varepsilon_{\max}}{\dot{\varepsilon}_{\mathrm{av}}} = \frac{0.1}{500} = 0.0002\,s = 0.2\,ms = 200\mu s$$

Quasi-static equilibrium contd

Wave propagation speed:

$$c = \sqrt{\frac{E}{\rho}}$$

Specimen length:

$$L$$

Wave travel time:

$$\Delta t = \frac{L}{c}$$

Example 2 (Aluminium sample L=1cm):

$$c = 5000\frac{m}{s}$$

$$L = 10mm$$

$$\Delta t = \frac{L}{c} = \frac{10}{5.10^6} = 2.10^{-6}s = 2\mu s$$

Principle of quasi–static equilibrium

For long time scale:

Duration of the experiment:

$$T = \frac{\varepsilon_{\mathrm{max}}}{\dot{\varepsilon}_{\mathrm{av}}}$$

For short time scale:

Time for the wave travel:

$$\Delta t = \frac{L}{c}$$

Quasi-static experiment – condition when testing elasto-plastic material:

$$F_{IN}(t) = F_{OUT}(t) \Leftrightarrow \Delta t \ll T$$

$$\boxed{\frac{L}{c} \ll \frac{\varepsilon_{\mathrm{max}}}{\dot{\varepsilon}_{\mathrm{av}}}} \tag{3}$$

Issues with: brittle materials (ceramics, $\varepsilon_{max} = 0.01$), soft materials (polymers, $c = 1000\frac{m}{s}$), coarse microstructure, e.g. metal foams, $L \gg 1mm$.

Dynamic equilibrium

Not valid test - ordnance gelatin, strain-rate $1000\,\mathrm{s}^{-1}$

- $F_{in} \neq F_{out}$
- No force convergence

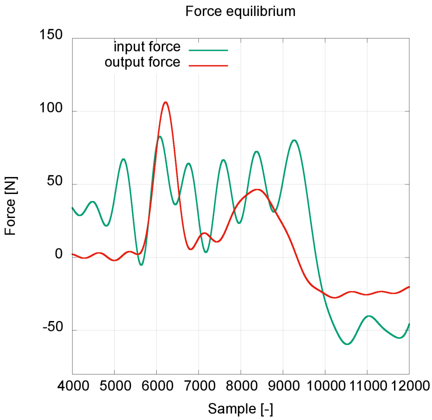

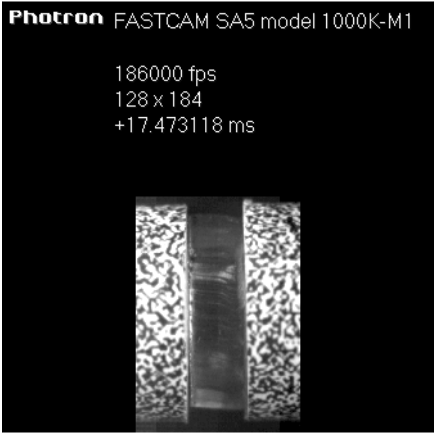

Dynamic equilibrium

Valid test - PP putty, strain-rate 2000 s^{-1}

- $F_{in} = F_{out}$
- Force convergence

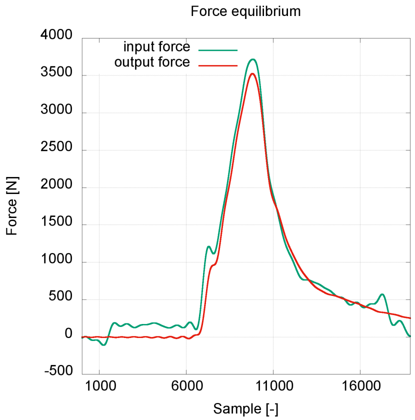

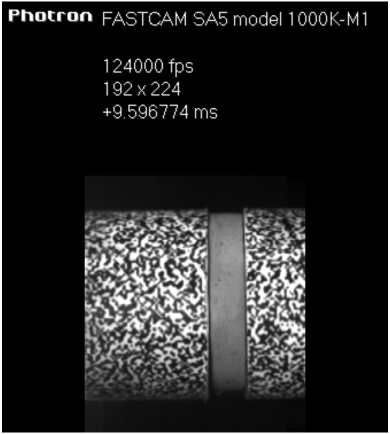

Auxetic materials

Auxetics

- negative Poisson's ratio
- cellular structure
- high energy absorption
- penetration resistant

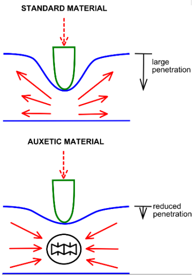

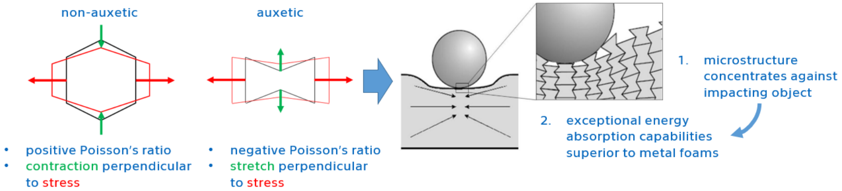

Experiments - Materials

Auxetic lattices

- 3 structure types
- 2D cut-missing-rib, 2D re-entrant, 3D re-entrant
- Additively manufactured using SLS
- Powdered 316L-0407 stainless steel
- $12 \times 12 \times 12\,\mathrm{mm}$

Pu/Ni hybrid foam

- A. Jung - Saarland University
- Polyurethane open-cell foam
- Nanocrystalline nickel electrodeposition coating
- Cost-effective material
- $\varnothing 20 \times 10(20)\,\mathrm{mm}$

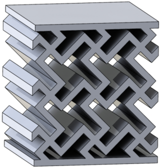
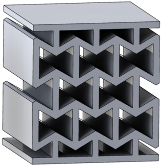
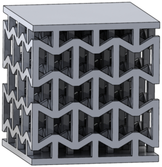
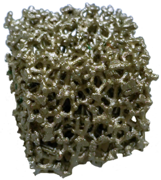

SHPB Experimental setup

Parameters

- Striker bar 200 – $500\,\mathrm{mm}$
- Impact velocity 5 – $35\,\mathrm{m/s}$
- Pulse-shaping
- High-speed camera
  $100,000 - 124,000\,\mathrm{fps}$

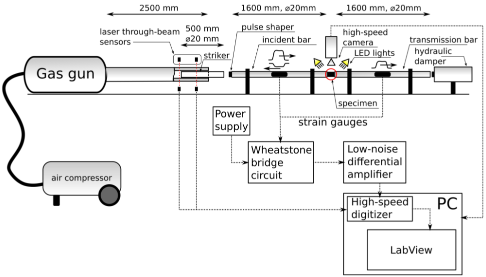

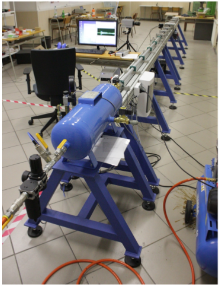

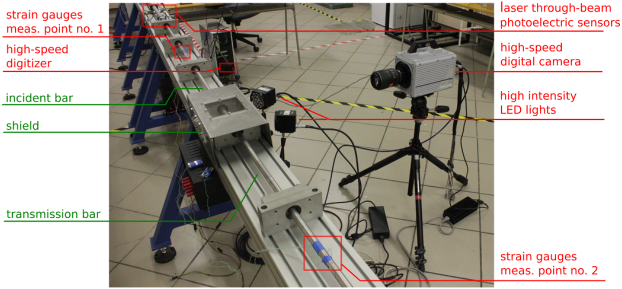

Digital image correlation (DIC)

- Optical measurement
- Custom DIC tool
- Lucas-Kanade tracking algorithm
- Displacement evaluation
- Strain evaluation

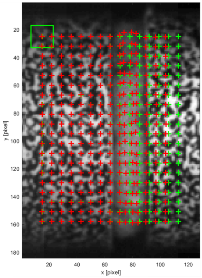

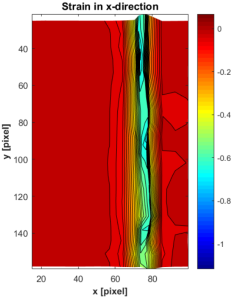

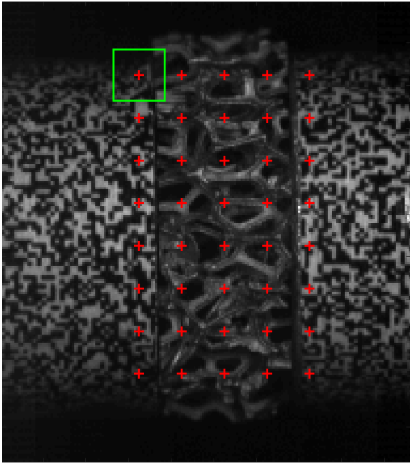

3D printed structures

Selective Laser sintering

- additive manufacturing technique
- uses a laser as the power source to sinter powdered material
- aiming the laser automatically at points in space defined by a 3D model
- binding the material together to create a solid structure

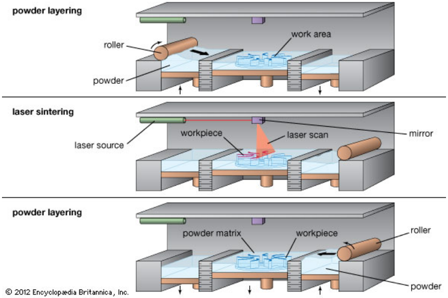

Auxetics

Metamaterials

- structures or materials that have a negative Poisson's ratio
- stretched, they become thicker perpendicular to the applied force
- due to their internal structure when the sample is uniaxially loaded
- auxetics can be single molecules, crystals, or macroscopic structure
- expected to have mechanical properties – high energy absorption and fracture resistance
- applications such as body armor, robust shock absorbing material

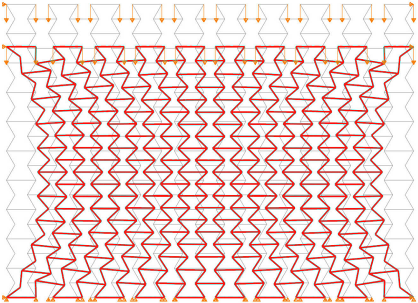

Auxetic materials

Auxetics

- negative Poisson's ratio
- cellular structure
- high energy absorption
- penetration resistant

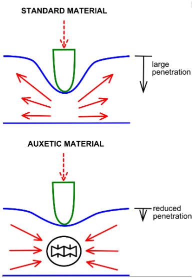

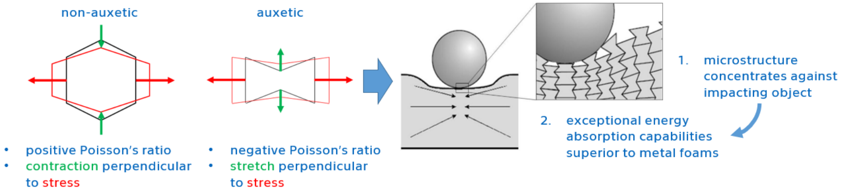

Experiments - Materials

Auxetic lattices

- 3 structure types
- 2D cut-missing-rib, 2D re-entrant, 3D re-entrant
- Additively manufactured using SLS
- Powdered 316L-0407 stainless steel
- $12 \times 12 \times 12\,\mathrm{mm}$

Pu/Ni hybrid foam

- A. Jung - Saarland University
- Polyurethane open-cell foam
- Nanocrystalline nickel electrodeposition coating
- Cost-effective material
- $\varnothing 20 \times 10(20)\,\mathrm{mm}$

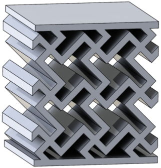
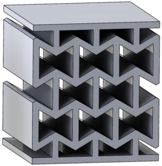
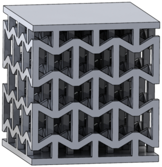
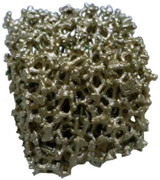

Illustrative DIC results - Auxetic lattices - different coating thickness

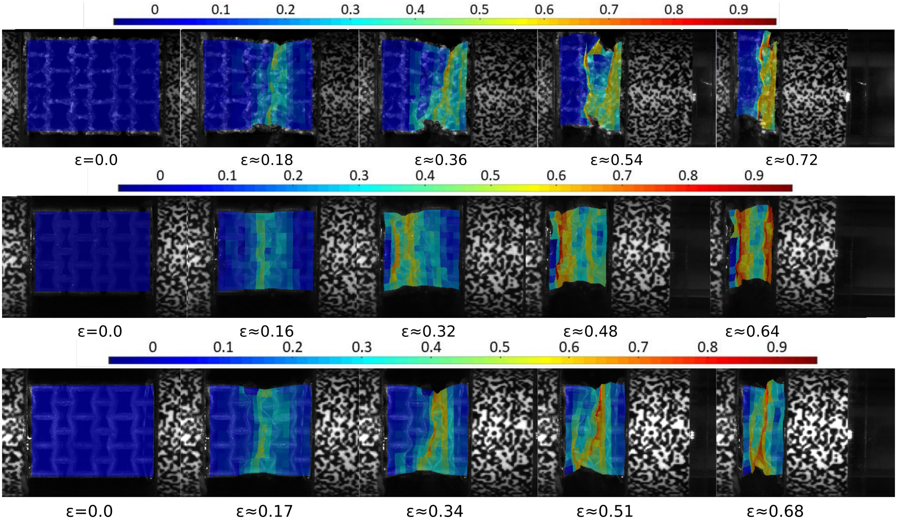

Displacements time evolution

2D reentrant structure AuxR - 60μm coating thickness

displacement u_x

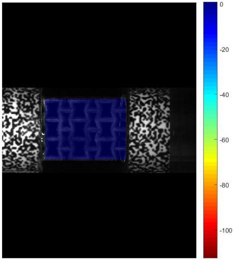

strain E_x

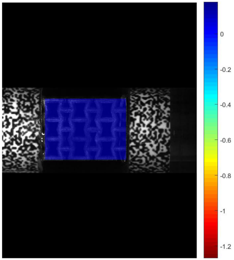

Displacements time evolution

2D reentrant structure AuxR - 120μm coating thickness

displacement u_x

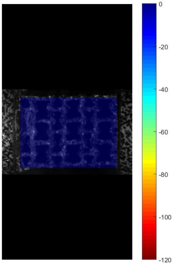

strain E_x

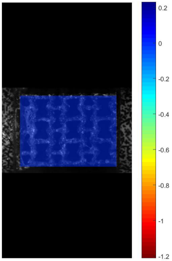

Results - Auxetic lattices

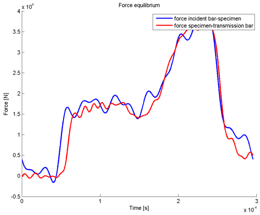

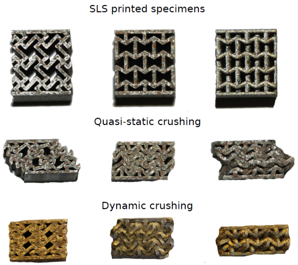

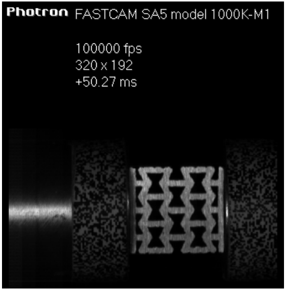

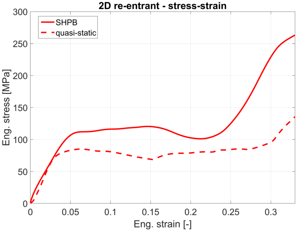

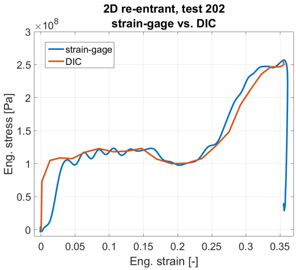

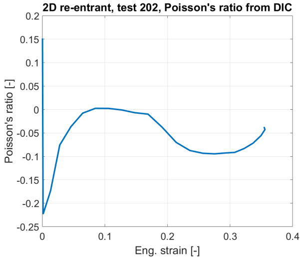

Hybrid foams testing

Pu/Ni hybrid foam

- polyurethane filter foam, pore size of 1.3*ppm* (pores per linear milimeter)
- electro coated with approx. $75\mu m$ nickel layer
- low density (approx. $800 kg/m^3$) and mechanical impedance
- energy absorption applications (traffic safety etc.)
- low cost production (polyuretane core)

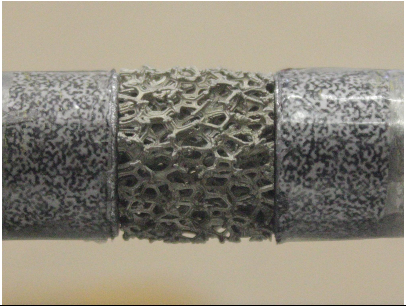

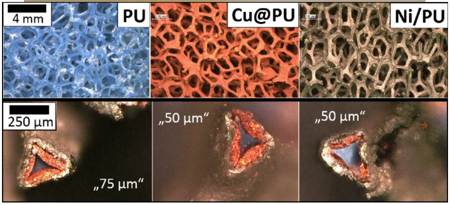

DIC Results

Experiment no. 270

- striker velocity: $v_s = 22.1 m/s$ (low strain-rate)
- sample diameter: $d = 22.4 mm$
- sample height: $l = 10.1 mm$

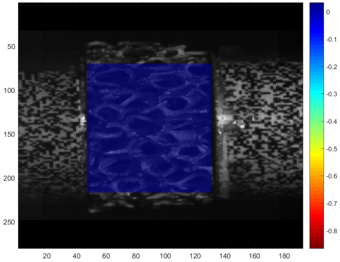

Experiment no. 317

- striker velocity: $v_s = 43.7 m/s$ (high strain-rate)
- sample diameter: $d = 21.8 mm$
- sample height: $l = 18.6 mm$

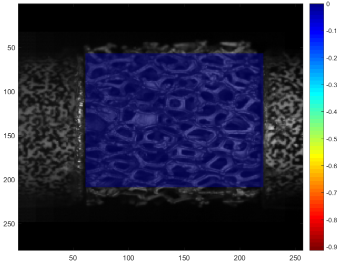

DIC and Strain-Gauge measurement comparison

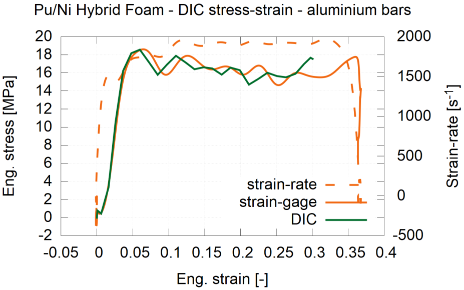

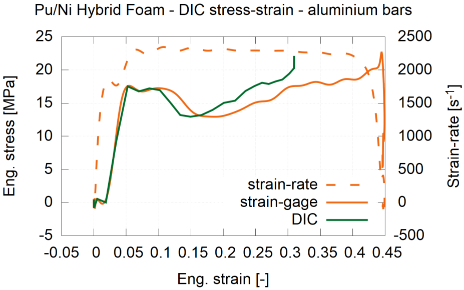

- good agreement between DIC and strain-gauge curves up to 30 % deformation
- sample size exceeds the measuring bars $\rightarrow$ loss of correlation of the parts outside the monitored area

Flash X-ray

Flash X-ray system

merging impact dynamics with X-ray methods

Actual limitations

In-situ computed tomography - **quasi-static loading only**, long exposure times

Impact testing and high speed imaging - **no view into the objects**

Flash X-ray system - lab-based method (no synchrotron or particle accelerator) to provide view inside the objects during impact in Hopkinson bar

pre-commissioned at FTS CTU in March 2021

Principle

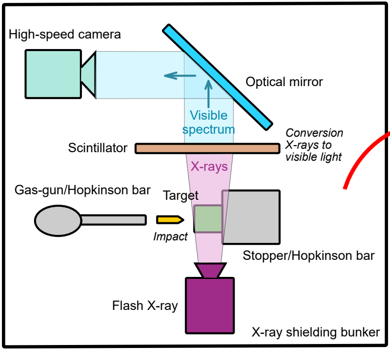

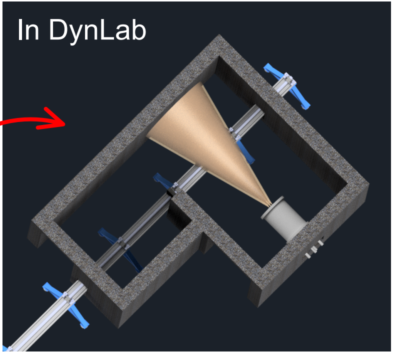

Flash X-ray system

merging impact dynamics with X-ray methods

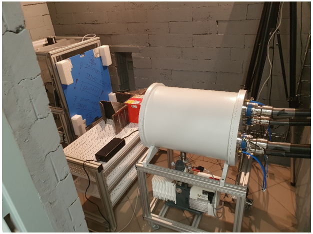

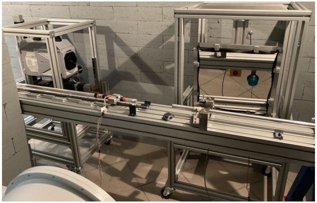

Pilot test

4 bursts per 0.01 ms, 20 ns exposure
high-speed imaging 100 kfps
chrome-vanadium tool

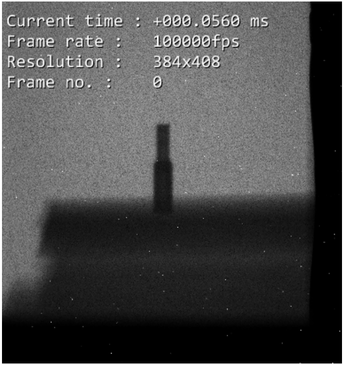

Flash X-ray imaging during impact

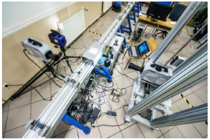

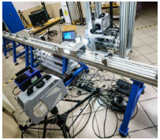

Extremely short exposure time X-ray pulse of 20 ns, 300 kV enables the study of dynamic events:

- OHPB / SHPB : impact velocity 20 – N100 m/s
- 2x Photron Fastcam SA-Z (2Mfps, 159 ns)

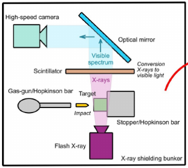

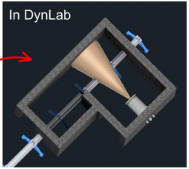

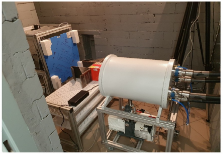

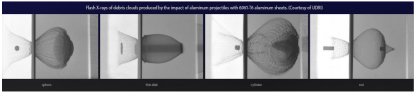

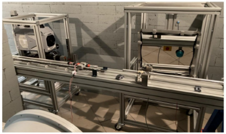

Thank you for your attention